

Bulk Termination of the Quasicrystalline Five-Fold Surface of $\text{Al}_{70}\text{Pd}_{21}\text{Mn}_9$

Z. Papadopolos* and G. Kasner

Institut für Theoretische Physik, Universität Magdeburg, PSF 4120, D-39016 Magdeburg, Germany

R.D. Diehl

Department of Physics, Pennsylvania State University, University Park, PA 16802, USA

J. Ledieu and R. McGrath

Surface Science Research Centre,

The University of Liverpool, Liverpool L69 3BX, UK

T.A. Lograsso and D.W. Delaney

Ames Laboratory, Iowa State University, Ames, IA 50011, USA

(Dated: December 2, 2024)

The structure of the $\text{Al}_{70}\text{Pd}_{21}\text{Mn}_9$ surface has been investigated using high resolution scanning tunnelling microscopy (STM), and an atomically resolved surface has been imaged. The location of this surface-plane has been estimated in the bulk model \mathcal{M} for icosahedral (i)-AlPdMn based on the three-dimensional tiling $T^{*(2F)}$ for an F-phase. The high resolution STM image of the surface allows the position of the bulk terminations to be fixed within the layers of Bergman polytopes in the model \mathcal{M} . They are 4.08 Å in the direction of the bulk from a surface of the most dense Bergman layers. The average atomic density of terminations consisting of two plane-layers at the new positions is consistent with the results of Gierer *et al.* From the coding window of the model (\mathcal{M})-termination-plane we estimate the shortest edge of a possible tiling by Penrose (P1) prototiles to be 7.8 Å. The experimentally derived tiling of the surface has edge length 8.0 ± 0.3 Å and hence matches edge-length expected from the model.

PACS numbers: 61.44.Br, 68.35.Bs, 68.37.Ef, 61.14.Hg

I. INTRODUCTION

More than ten years ago, the discovery that centimetre size samples of decagonal (*d*)-AlCuCo and icosahedral (*i*)-AlPdMn could be grown opened up the possibility of surface studies of these quasicrystals¹. Since then other quasicrystal samples have been grown to similar dimensions. To date, most studies have been performed on the five-fold surface of $\text{Al}_{70}\text{Pd}_{21}\text{Mn}_9$ ^{2,3,4,5,6,7,8,9,10,11,12,13,14}. A consensus has emerged from these studies that this surface, after fairly standard ultra-high-vacuum (UHV) sputtering and annealing procedures, is itself quasicrystalline. In this work we attempt to address these questions, and using a combined experimental and theoretical approach, we show that this surface can be considered to be a termination of the known bulk structure^{15,16,17,18,19,20,21}.

The dynamical low-energy electron diffraction (LEED) analysis carried out by Gierer *et al.* indicated that the fivefold surface of the $\text{Al}_{70}\text{Pd}_{21}\text{Mn}_9$ quasicrystal retained the bulk quasicrystallinity^{13,14}. X-ray photoelectron diffraction (XPD) studies are also consistent with a quasicrystalline surface nature^{10,11,12}. Large flat terraces may be produced, and scanning tunnelling microscopy

(STM) studies have presented similar images of the quasicrystalline surface^{2,3,4,5,7,8,9}. Schaub *et al.*^{2,3,4,5} produced detailed STM images of the terraces that reveal a dense distribution of *dark pentagonal holes* of edge length circa 4.8 Å oriented parallel to each other, together with a more random distribution of bright protrusions. They correlated the measurements between structural elements both within the terraces and across steps on the surface. Later, we demonstrated a correspondence of these measurements with the geometric model \mathcal{M} ^{19,20,21} for atomic positions of an F-phase²². The model \mathcal{M} is based on the three-dimensional icosahedral tiling $T^{*(2F)}$ ²³ decorated essentially by Bergman/Mackay polytopes^{16,17,18,24}. The observed terrace structure of the surface was explained in terms of the layer structure of the bulk model. The dark pentagons observed on the surface corresponded with the Bergman polytopes³⁹ in the bulk layers. The position of a given type of terrace was matched to a layer characterised by a density of certain Bergman polytopes and their distribution pattern. We assumed that the surface termination respects the integrity of the Bergman polytopes as clusters, at least in the most dense layers, and we supposed that such a layer of Bergman polytopes is exactly below the termination. However, under these assumptions it was not possible to explain the observed edge length (circa 4.8 Å) of the dark pentagonal holes, as this was bigger by the factor $\tau = (\sqrt{5} + 1)/2$ than the pentagonal surfaces of the Bergman polytope (circa 3 Å)¹⁹.

*Author for correspondence: Phone: +49 7071 29 76378; Fax: +49 7071 29 5604; e-mail: zorka.papadopolos@uni-tuebingen.de

Later Shen *et al.*, using an autocorrelation analysis showed that the surface structure is consistent with a bulk structure based on truncated pseudo-Mackay icosahedra or Bergman clusters⁷.

A fundamental limitation of those STM studies was that the resolution of the images, while sub-nanometre, was not atomic. Therefore direct comparison with bulk models was not straightforward. Additionally, the presence of bright protrusions disrupted any attempted tiling, and so comparison with tiling models was not possible. In this study, we have improved upon our previous sample preparation technique. This has led to a more perfect surface devoid of the protrusions (section III), and this in turn has led to improved resolution in the STM images. The better resolution, together with the structural perfection, allows us to demonstrate that the surface structure is consistent with a bulk termination²⁵, using the bulk model of Boudard *et al.*¹⁵. Furthermore, the experimental tiling of the plane matches with the tiling $\mathcal{T}^{*((P1)^r)}$, derived from the tiling $\mathcal{T}^{*(2F)}$ (sections II and IV).

Due to the atomically resolved images of the surface we are able to fix the bulk termination to be 4.08 Å deeper within the layer of Bergman polytopes (section IV) than we expected in Ref.¹⁹. In this new position of the termination, the edge length of the dark pentagonal holes observed by Schaub *et al.*¹⁹ is now understood (section IV). Moreover we conclude that the termination is maximally dense in dark pentagonal holes that we can now interpret as *dissected* Bergman polytopes. The average density of the atomic positions in terminations on these new positions is in agreement with the one determined by Gierer *et al.*¹⁴ (section IV B).

II. THEORETICAL BACKGROUND

A geometric model \mathcal{M} for the atomic positions of i-AlPdMn or i-AlCuFe^{17,18} has been used to interpret the STM measurements data of Schaub *et al.*^{2,4} on the five-fold surfaces of i-AlPdMn^{19,20}. In the model \mathcal{M} , the F -phase²² three-dimensional tiling $\mathcal{T}^{*(2F)}$ ²³ is decorated by Bergman (and automatically Mackay) polytopes^{17,18}. For details on Bergman and Mackay polytopes, see Ref.¹⁶. The geometric model is based on the Katz-Gratias model²⁴ that is explained by Elser¹⁶ in a three-dimensional “parallel space”, \mathbb{E}_{\parallel} , the space in which the model projected from D_6 lattice^{22,26} exists. The atoms of i-AlPdMn²⁷ or of i-AlCuFe²⁴ can be placed on three translational classes of atomic positions with respect to the D_6 -lattice, and are denoted by $q_{D_6} \equiv q$, b and a , see Table I in section IV and Ref.²⁰. These atomic positions in \mathbb{E}_{\parallel} are coded by the corresponding “windows” or “acceptance domains” in three-dimensional “perpendicular space”, \mathbb{E}_{\perp} . Note that the six-dimensional D_6 lattice, that after Mermin *et al.*²² model an F -phase, acts in the six-dimensional space that is a sum of \mathbb{E}_{\parallel} and \mathbb{E}_{\perp} . These windows in \mathbb{E}_{\perp} are denoted by W_q , W_b

and W_a , respectively. The windows for the model \mathcal{M} were constructed in Refs.^{17,18,20}. The tiling $\mathcal{T}^{*(2F)}$ defines the quasiperiodic structure. More accurately, the model \mathcal{M} is supported by $\tau\mathcal{T}^{*(2F)}$, the tiling $\mathcal{T}^{*(2F)}$ scaled by the factor $\tau = (\sqrt{5} + 1)/2$. The quasilattice points of $\tau\mathcal{T}^{*(2F)}$ are in the class of $q \in D_6$. All points of the related quasilattice (vertices of the tiling) can be embedded in a sequence of planes orthogonal to the five-fold symmetry axis of an icosahedron (“five-fold direction”). The planes orthogonal to the axis are the “five-fold planes”. The sequence of planes forms a “decorated Fibonacci sequence” with separations $s(\text{hort})$, $m(\text{edium})$, $l(\text{ong})$ ($l = \tau m = \tau^2 s$), see Fig. 12(a) in Section IV. This sequence contains a Fibonacci sequence with intervals m and l as a subsequence. For i-AlPdMn the standard distance parallel to the five-fold direction is $\mathfrak{G} = 4.56$ Å, and $s = \left(\frac{2}{\tau+2}\right) \mathfrak{G} = 2.52$ Å, $m = \tau \left(\frac{2}{\tau+2}\right) \mathfrak{G} = 4.08$ Å, $l = \tau^2 \left(\frac{2}{\tau+2}\right) \mathfrak{G} = 6.60$ Å. The planes in the sequence have been classified into five types, see¹⁹. In the planes of type 1 a quasiperiodic tiling $\mathcal{T}^{*(A_4)}$ ²⁸ appears^{19,29} scaled by a factor τ . In the planes of type 2, 3 and 4 there appear the fragments of the same tiling of a plane by golden triangles (see Ref.¹⁹, Fig. 7) with the same inflation properties as in the tiling $\mathcal{T}^{*(A_4)}$ ^{28,29}. The planes of type 1 to 4 are ordered in the Fibonacci sequence mentioned above.

In Refs.^{19,21} the model is compared to the ideal icosahedral monograins under the assumption that the terraces on the surface of the material are like the planes in the bulk, i. e. not reconstructed. This we will also assume in this paper. The terraces observed by Schaub *et al.*^{2,4} were related to the sequence of the planes of the model \mathcal{M} described above, see also Ref.¹⁹. Whereas Schaub *et al.*, after annealing at $\approx 800^\circ\text{C}$ observed only Fibonacci ordered step heights m and l on the surface^{2,4}, Shen *et al.*, after annealing at $\approx 630^\circ\text{C}$ detected also the step height s^7 .

In this paper we study the fine structure within the observed terraces and compare it to the geometric model \mathcal{M} ¹⁹. Whereas in¹⁹ we succeeded in relating the sequence of the terrace-like five-fold surfaces of Schaub^{2,4} to the layers of the Bergman polytopes in the geometric model \mathcal{M} , in this paper, using the high resolution STM images of a five-fold surface we will fix the position of the planes within the layers of Bergman polytopes.

In order to recognise and identify the fine structure of the observed surface, we consider certain tilings in the five-fold planes and a covering with the set of prototiles among which are the pentagons and pentagonal stars⁴⁰. These tilings will be locally derived from the tiling $\mathcal{T}^{*(A_4)}$. The local derivation will be to a certain stage exact, and thereafter, random. The tiling $\mathcal{T}^{*(A_4)}$ scaled by the factor τ defines the quasiperiodic structure of the planes on the surfaces according to the model \mathcal{M} introduced above¹⁹. The prototiles in the tiling $\mathcal{T}^{*(A_4)}$ are golden triangles. The edges of the triangles in the tiling are parallel to the two-fold symmetry axes

of an icosahedron (“two-fold directions”) and are of two lengths, $\mathbb{2}$ and $\tau\mathbb{2}$. The three-dimensional model \mathcal{M} is supported by the tiling $\tau\mathcal{T}^{*(2F)}$ and consequently in the five-fold surfaces by $\tau\mathcal{T}^{*(A_4)}$. Hence the edges are $\tau\mathbb{2}$ and $\tau^2\mathbb{2}$. With the standard value $\mathbb{2} = 4.795 \text{ \AA}$ in the case of i-AlPdMn, $\tau\mathbb{2} = 7.758 \text{ \AA}$ and $\tau^2\mathbb{2} = 12.553 \text{ \AA}$.

The structure on the surface observed by STM can be tiled uniquely only if the tiling, as an abstract structure, is derivable from the set of quasilattice points, and if the rules of the local derivation are defined on relatively small distances with respect to the area of an observed surface.

A. Local Derivations of Tilings and Coverings Containing Pentagonal Prototiles from the Tiling $\mathcal{T}^{*(A_4)}$

As an intermediate step we locally derive the tiling \mathcal{T}^* with pentagon, acute rhombus and hexagon as prototiles from the quasilattice $\mathcal{T}^{*(A_4)}$, as shown in Fig. 1. The tiling has an inflation factor τ . It is clear that the tiling \mathcal{T}^* can be reconstructed from its own quasilattice points. All edges of the prototiles in \mathcal{T}^* are of length $\tau\mathbb{2}$. In the geometric model \mathcal{M} the prototiles are augmented by a factor τ , so the edge length is $\tau^2\mathbb{2} = 12.553 \text{ \AA}$. All prototiles of \mathcal{T}^* are the unions of golden triangles of the previous tiling $\mathcal{T}^{*(A_4)}$, as shown in Fig. 1. If we keep that content, the window for the tiling is identical to the window for $\mathcal{T}^{*(A_4)}$ (because none of the vertex (quasilattice) points is omitted). Small fractions of the tiling \mathcal{T}^* have been observed in the five-fold surfaces of the decagonal (d)-AlCuCo³⁰.

From the intermediate tiling \mathcal{T}^* we can locally derive a *covering* of the tiling $\mathcal{T}^{*(A_4)}$. This covering is by two cells in a shape of pentagons, the smaller one, D_{\parallel}^a , of edge length $\mathbb{2}$ and the bigger, D_{\parallel}^b , of edge length $\tau\mathbb{2}$, see Fig. 3(a). Let us denote this covering of the tiling $\mathcal{T}^{*(A_4)}$ by $\mathcal{C}_{\mathcal{T}^{*(A_4)}}^s$. Each acute rhombus from \mathcal{T}^* is transformed into a pair of pentagons of edge length $\mathbb{2}$ (shown at the lefthand side of Fig. 3(a)), and each hexagon is transformed into a pair of overlapping pentagons of edge length $\tau\mathbb{2}$ (at the righthand side of Fig. 3(a)). The remainder of the tiling $\mathcal{T}^{*(A_4)}$ should be covered by pentagons of edge length $\tau\mathbb{2}$ as in the tiling \mathcal{T}^* , see Fig. 1. The above-defined covering $\mathcal{C}_{\mathcal{T}^{*(A_4)}}^s$ of the tiling $\mathcal{T}^{*(A_4)}$ is a sub-covering of the covering of Kramer^{31,32}. Kramer covers the tiling $\mathcal{T}^{*(A_4)}$ also by two pentagons of the same size as above. These cells are in \mathbb{E}_{\parallel} projected Delone cells D^a and D^b of the lattice A_4 . In \mathbb{E}_{\parallel} they are denoted by D_{\parallel}^a and D_{\parallel}^b , respectively. Let us denote the Kramer’s covering by the symbol $\mathcal{C}_{\mathcal{T}^{*(A_4)}}^K$. The set of pentagons in $\mathcal{C}_{\mathcal{T}^{*(A_4)}}^s$ of edge length $\tau\mathbb{2}$ is identical to the set of D_{\parallel}^b ’s in $\mathcal{C}_{\mathcal{T}^{*(A_4)}}^K$. The set of pentagons in $\mathcal{C}_{\mathcal{T}^{*(A_4)}}^s$ of edge length $\mathbb{2}$, derived from the acute rhombuses, is a *subset* of the set of all D_{\parallel}^a ’s in $\mathcal{C}_{\mathcal{T}^{*(A_4)}}^K$, and *therefore* is the covering $\mathcal{C}_{\mathcal{T}^{*(A_4)}}^s$ of $\mathcal{T}^{*(A_4)}$ a *subcovering* of the

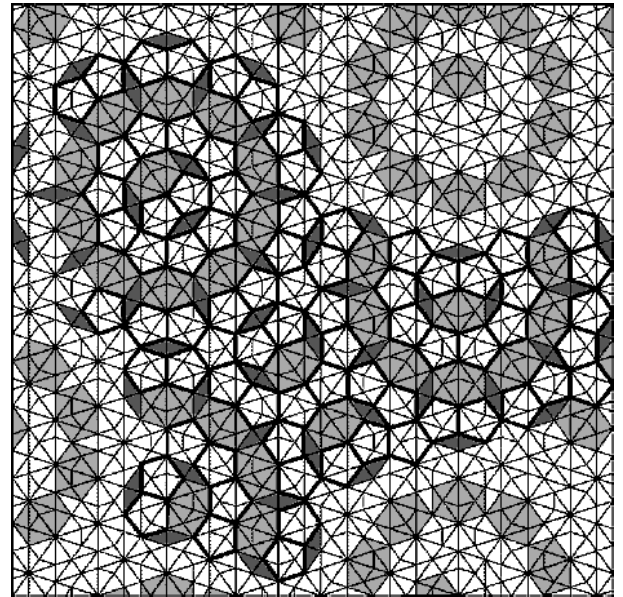


FIG. 1: The tiling \mathcal{T}^* of the plane by the acute rhombus, pentagon and hexagon as the prototiles. The tiles are marked by thick lines and different gray shadows. The tiling $\mathcal{T}^{*(A_4)}$, from which \mathcal{T}^* is locally derived, is shown in background using thin lines.

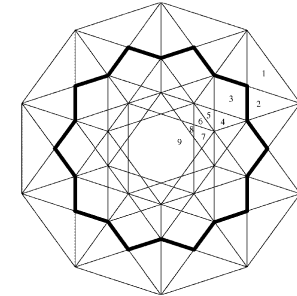


FIG. 2: The coding window for the tiling \mathcal{T}^* , without the content of golden triangles, is inscribed by thick lines in decagon, the coding window for the tiling $\mathcal{T}^{*(A_4)}$. The codings of the 9 types of vertex configurations in the tiling $\mathcal{T}^{*(A_4)}$ are marked by the numbers 1-9.

covering $\mathcal{C}_{\mathcal{T}^{*(A_4)}}^K$ ^{31,32}. Whereas the decking coefficient of $\mathcal{C}_{\mathcal{T}^{*(A_4)}}^K$ is $d^K = 3 - \tau \approx 1.382$, the decking coefficient of sub-covering $\mathcal{C}_{\mathcal{T}^{*(A_4)}}^s$ is $d^s = 2\tau - 2 \approx 1.236 < 1.382$. For the decking coefficient see Ref. ³³. In the subcovering $\mathcal{C}_{\mathcal{T}^{*(A_4)}}^s$ only the single and double decking of the tiles by the covering clusters are present. The triple decking, which exists in the covering $\mathcal{C}_{\mathcal{T}^{*(A_4)}}^K$ is excluded³³ in $\mathcal{C}_{\mathcal{T}^{*(A_4)}}^s$. The window for the sub-covering $\mathcal{C}_{\mathcal{T}^{*(A_4)}}^s$ of $\mathcal{T}^{*(A_4)}$ by two pentagons *without* the content of golden triangles is presented in Fig. 4.

From the tiling \mathcal{T}^* let us keep all acute rhombuses, and replace each hexagon by two overlapping pentagons (as in

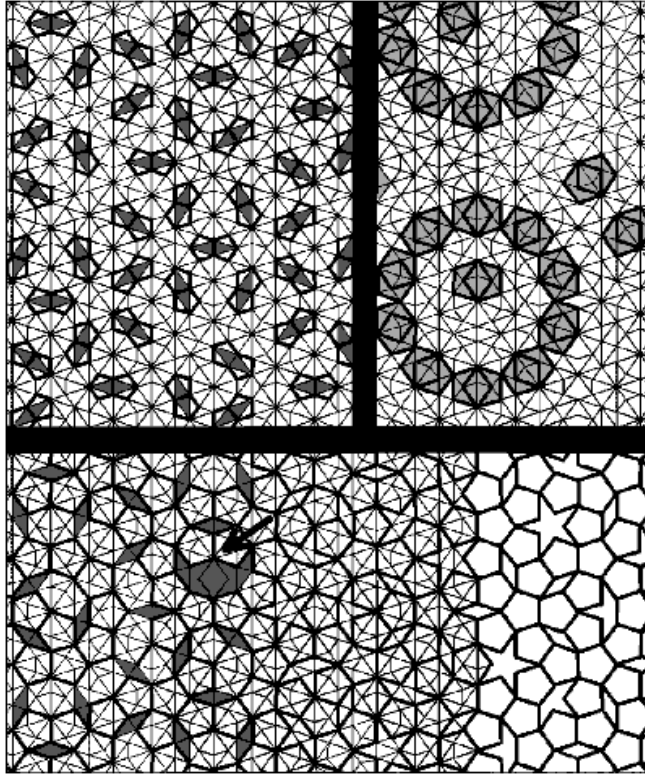


FIG. 3: (a) The derivation $T^* \rightarrow C_{T^*(A_4)}^s$ is in *upper* part of the figure; (b) $T^* \rightarrow T^{*((P1)r)}$ is in *lower* part of the figure.

the sub-covering $C_{T^*(A_4)}^s$). This is an exact local derivation, see the lefthand side of Fig. 3(b). At this stage we *randomly* choose one of the pentagons from each overlapping pair, and the rest of each hexagon unites with the neighboring acute rhombus. In this way, either a crown or a pentagonal star appears to replace the rhombus, and we obtain a partly random tiling $T^{*((P1)r)}$, see the righthand side of the Fig. 3(b). The ideal class of tilings $(P1)$ with the inflation factor τ are described in Refs.^{34,35}. In Fig. 5(a), the window that exactly defines the quasilattice of the tiling $T^{*(P1)}$ is inscribed in the window of the tiling $T^*(A_4)$.

There is another tiling of a plane by pentagonal stars, pentagons and obtuse rhombuses introduced by Niizeki³⁵. Let us call it the Niizeki star-tiling and denote it by $T^{*(Ns)}$. The inflation factor of this tiling is also τ . In Fig. 6 we derive this tiling from the tiling T^* . In Fig. 6(a) (upper part of the Fig. 6) on the lefthand side, from the set of all stars, only the locally derivable stars are presented. The locally derivable star appears wherever there exists an acute rhombus neighboring one or two hexagons, each by an edge. Between these stars, there appear obtuse rhombuses. In Fig. 6(a) on the righthand side the white spaces around the isolated acute rhombuses are framed by thick lines. Inside these patches, there appear pairs of overlapping stars, inscribed in one single place in the figure and marked by an arrow. Their

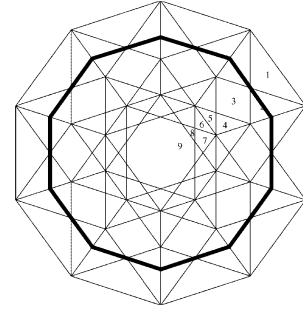


FIG. 4: The window for the covering $C_{T^*(A_4)}^s$ without the content of golden triangles, inscribed by the thick lines in the window of the tiling $T^*(A_4)$.

overlap is exactly the acute rhombus. Up to the choice of one star from each pair of overlapping stars, the local derivation of the tiling is exact. The exact tiling of the plane by the stars, obtuse rhombuses and pentagons, $T^{*(Ns)}$, is uniquely determined by its window inscribed in the window of $T^*(A_4)$, see Fig. 5(b). It is the window of Niizeki tiling. We choose *randomly* a star from each overlapping pair of stars indicated in the lower part of Fig. 6 and obtain a partly random tiling $T^{*((Ns)r)}$. The only edge length that appears in the tiling is $\tau\mathcal{R}$ (in the geometric model \mathcal{M} , it is $\tau^2\mathcal{R} = 12.553 \text{ \AA}$). It is also the tiling that could be eventually seen/reconstructed from the STM images of the surfaces orthogonal to the five-fold direction by i-AlPdMn and i-AlCuFe. Also by a decagonal phase.

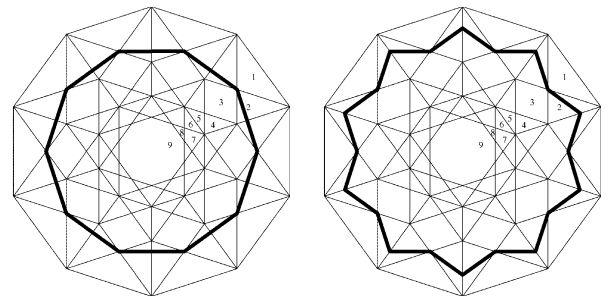


FIG. 5: (a) The window for $T^{*(P1)}$ is inscribed in the window for $T^*(A_4)$ by thick lines. (b) The exact tiling of the plane by the stars, obtuse rhombuses and pentagons, $T^{*(Ns)}$, is uniquely determined by its window inscribed by thick lines in the window of $T^*(A_4)$. It is the window that is coding the Niizeki tiling $T^{*(Ns)}$.

Both exact tilings, $T^{*(P1)}$ and $T^{*(Ns)}$, can be locally derived from their respective quasilattice points. In the reconstruction of tiling $T^{*(P1)}$ and $T^{*(Ns)}$ from the respective quasilattices there appear: (i) pairs of pentagonal sets of points centered in each other and mutually rotated by $2\pi/10$. The set of points of the smaller size

(the smallest pentagonal set in the tiling) is on the neighboring distances ②, the bigger, on neighboring distances $\tau^2 ②$. Each pair leads to the pentagonal star; (ii) the isolated pentagonal sets with neighboring distances $\tau ②$ are to be connected in pentagons. In order to reconstruct the tiling $\mathcal{T}^{*(P1)}$, it is enough to draw the pentagons from the isolated five-tuples of symmetrically ordered points. In order to reconstruct the tiling $\mathcal{T}^{*(Ns)}$ one draws the stars from the pairs of pentagonal sets. One can show that in an abstract sense the tilings $\mathcal{T}^{*(P1)}$ and $\mathcal{T}^{*(Ns)}$ can be mapped one-to-one to each other³³. If we consider an experimental five-fold surface atomically resolved, and tile the observed surface, we have first to identify the surface by a model plane, \mathcal{M} -plane. Then we determine the coding window for the plane in \mathbb{E}_\perp , the \mathcal{M} -plane window, and we place the biggest possible window of an exact tiling $\mathcal{T}^{*(P1)}$ or $\mathcal{T}^{*(Ns)}$ in the \mathcal{M} -plane window. Along this line, in section IV A we will determine the edge length of a possible tiling of an observed surface by the prototiles of the tiling P1.

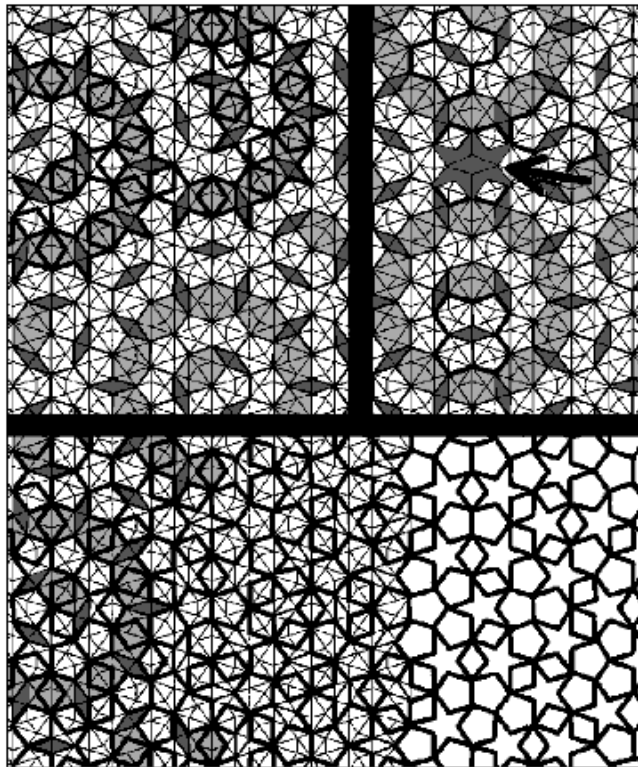


FIG. 6: Local derivation: $\mathcal{T}^* \longrightarrow \mathcal{T}^{*((Ns)^r)}$.

III. EXPERIMENT DETAILS AND RESULTS

A. Experimental Details

The quasicrystal sample was grown at Ames Laboratory using the Bridgman method^{36,37}. After being cut

perpendicular to its five-fold symmetry axis in air, the sample surfaces were prepared²⁵ by mechanical polishing using 6, 1 and 1/4 μm grit diamond paste on Kemet cloth (PSU-M type for the 6 μm and NMH type for the other grit sizes) for one hour. The surface was subsequently prepared in ultra-high vacuum (UHV) by sputtering it with 0.5 keV Ar ions, with a sputtering angle of 20°-30° relative to the surface parallel, followed by annealing to 970 K for two hours. The Auger electron spectroscopy (AES) scans were taken in a different chamber, but following the same preparations sequence.

B. Experimental Results

The LEED pattern obtained from the surface has very sharp diffraction spots, a low background, and five-fold rotational symmetry (see Fig. 7(a)). High-resolution STM images from this surface exhibited flat terraces and atomic resolution (Fig. 7(c) and (d)). Fig. 7(b) shows an image of the surface where the preparation procedure was not optimized. The bright spots in this image correspond to protrusions of height up to 2.0 \AA , while dark spots are associated with holes of depth estimated to at least 1.5 \AA . This STM image is comparable to those in the work of Schaub *et al.*^{2,3,4,5}. The step heights measured from this image are comparable to those measured by Schaub *et al.*^{2,3,4,5}. Attempts to tile such images result in an incomplete tiling due to the interference of the large protrusions⁸.

When the surface preparation is optimized, large areas of the terraces have no protrusions, and the apparent corrugation within the terraces is $< 1\text{\AA}$. Because the STM tip can scan the surface more closely, it is possible to obtain higher resolution images. Fig. 7(d) shows a 100 $\text{\AA} \times 100 \text{\AA}$ high resolution STM image of one terrace. The features in this image are typical of atomic sizes (2-3 \AA). Larger features (4-6 \AA) are also evident and are probably clusters of a few atoms. Five-fold depressions are observed, as before, now in a shape of stars, and are indicated on Fig. 8(a). Pentagonal stars have the same orientation and each star can be framed in a pentagon of an edge-length $4.8 \pm 0.2 \text{\AA}$. In the inset present on Fig. 8(b), a fast Fourier transform (FFT) has been calculated for the high resolution STM image shown in Fig. 8(a) and this exhibits ten-fold symmetry, consistent with five-fold or ten-fold symmetry of the surface structure.

An even higher resolution image of the same surface is shown in Fig. 8(b). Several pentagons of edge length $8.0 \pm 0.30 \text{\AA}$ are outlined in this figure. Similar pentagons are found across the surface, with different features visible in their centers in some cases. Fig. 9(a) shows a full tiling of the high resolution STM image shown in Fig. 7(d)). In addition to pentagons, rhombuses, crowns and five-fold stars are evident. In contrast to the attempted tilings of the surface shown in Fig. 7(b), this tiling is continuous because there are no protrusions.

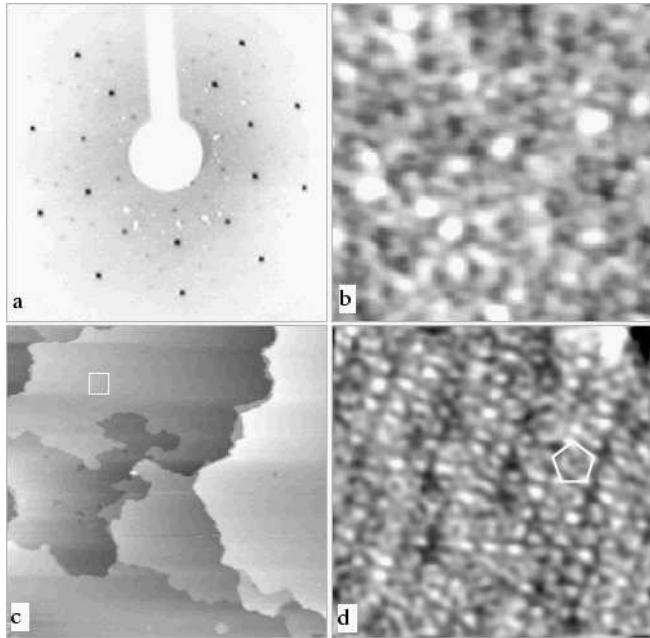


FIG. 7: (a) LEED pattern (inverted for clarity; 75 eV beam energy) recorded after annealing to 970 K. (b) $100 \text{ \AA} \times 100 \text{ \AA}$ STM image of a flat terrace from a non-optimal surface (bias voltage 2.29 V, tip current 0.59 nA). (c) $1500 \text{ \AA} \times 1500 \text{ \AA}$ STM image showing atomically flat terraces. A $100 \text{ \AA} \times 100 \text{ \AA}$ frame has been drawn on the largest terrace to emphasize the resolution of the following images. (d) $100 \text{ \AA} \times 100 \text{ \AA}$ high resolution STM image obtained on the five-fold surface using optimized preparation ($V=1 \text{ V}$, $I= 0.3 \text{ nA}$).

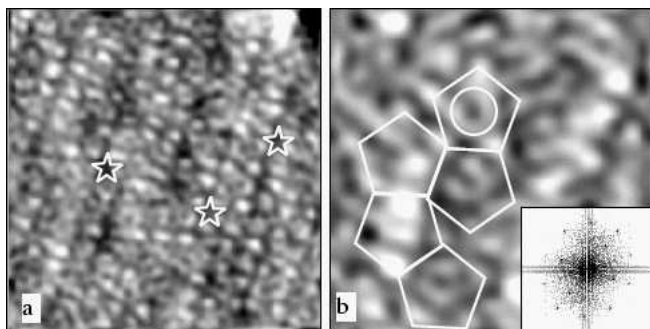


FIG. 8: (a) $100 \text{ \AA} \times 100 \text{ \AA}$ high resolution STM image obtained on the five-fold surface (same as Fig. 7(d)). Three pentagonal holes (stars) have been outlined. (b) $50 \text{ \AA} \times 50 \text{ \AA}$ high resolution STM image ($V= 1 \text{ V}$, $I= 0.3 \text{ nA}$) with several pentagons outlined. The FFT (inset) has ten-fold symmetry.

C. Comparison Between the Surface Observed by STM and Boudard's Model

In order to compare these results with bulk models, a dense atomic plane perpendicular to the five-fold axes of the *i*-AlPdMn quasicrystal has been chosen from Boudard's model¹⁵. The tiling shown in Fig. 9(a) is su-

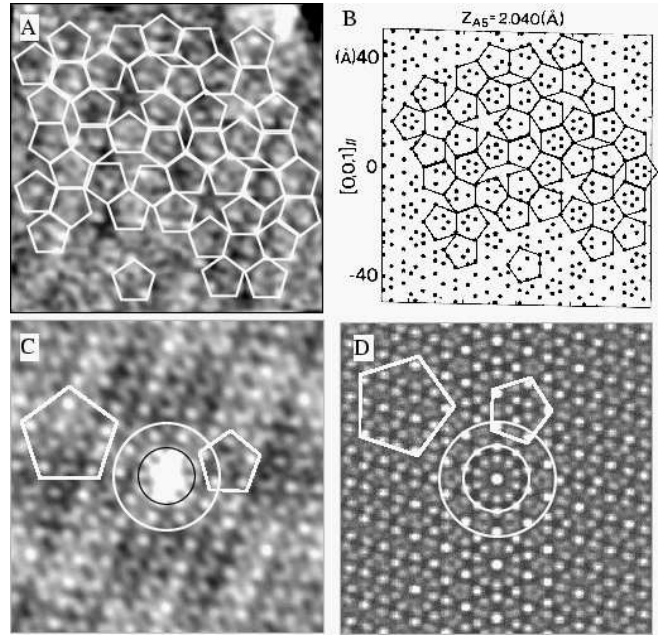


FIG. 9: (a) Experimental tiling of the high resolution STM image of Fig. 8(a). (b) Tiling obtained from the previous image superimposed on a dense atomic plane perpendicular to a five-fold axis from the model of Boudard *et al.*¹⁵. (c) $78 \text{ \AA} \times 78 \text{ \AA}$ lateral autocorrelation function of the STM iamge of Fig. 8(a). (d) $74 \text{ \AA} \times 74 \text{ \AA}$ lateral autocorrelation function of Boudard's model shown in Fig. 9(b).

perimposed on Boudard's plane and an excellent match is obtained in Fig. 9(b). None of the other 5 planes from ref.¹⁵ match this tiling. Several pentagons on Fig. 9(b) appear identical in that their centres contain five atoms forming an even smaller pentagon of edge length measured circa 3.0 \AA as shown on Fig. 10(c). These identical pentagons can be compared with the one outlined on Fig. 10(a). It is pointed out on Fig. 10(b) and (d) that the centres of the pentagons can differ (4 atoms in the centre in this case). The absence of atoms in the centre of the two large stars present on Fig. 9(b) is reflected in Fig. 9(a) by dark patches at the same positions. It is possible that tiling could be superimposed on the same plane with another orientation, and this analysis does not claim to give the exact atomic positions at the surface.

Among the tools available for image analysis, autocorrelation represents one of the most important methods when comparing models to STM data from aperiodic surfaces. Two-dimensional autocorrelations have been calculated for the high resolution STM image of Fig. 7(d) and for Boudard's plane (Fig. 9(b)); these are shown on Fig. 9(c) and Fig. 9(d) respectively. The symmetry of both autocorrelations is identical. The correlation maxima extend to long distances (near to the edges of Fig. 9(c),(d)) indicating a high degree of quasiperiodic order. The match between these two autocorrelation patterns is excellent. For comparison purposes, a ring and

two pentagons are outlined on both representations. The maxima present inside these patterns are very similar on both figures.

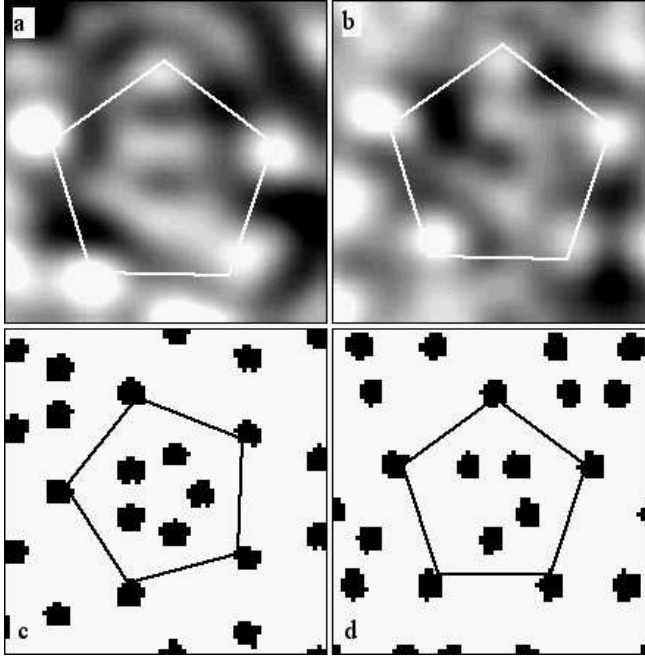


FIG. 10: (a), (b) Pentagons observed on the STM images. The atomic structures of their centres appears different. (c), (d) Pentagons obtained from the atomic plane presented in Fig. 9(b) (Boudard's model). Five atoms forming a smaller inner pentagon can be seen on Fig. (c) while only four are present on Fig. (d). The size of each figure is around $20 \text{ \AA} \times 20 \text{ \AA}$.

For a more quantitative comparison of Fig. 9(c) and Fig. 9(d), radial distribution functions have been calculated in both cases. The procedure consists of dividing the 360° around the centre of the autocorrelation function in 3000 increments. Along each line corresponding to each increment, the distances from the centre to the maxima are measured. All the measurements are then averaged and plotted as histograms (Fig. 11). Fig. 11(a) corresponds to the radial distribution function calculated from the high resolution STM image shown on Fig. 8(a). Maxima are found at $7.0, 12.0, 15, 19.5, 24, 27, 31.1$ and 38.4 \AA ($\pm 0.3 \text{ \AA}$). The radial distribution function calculated from Boudard's model (shown in 11(b)) is very similar, the main differences being the resolution of the peak at 15 \AA , the peak at 17 \AA and the splitting of the peaks at 34.8 \AA and 38.6 \AA . In contrast, only three maxima at $12, 21.8$ and 32.8 \AA appear on the radial distribution obtained from Fig. 11(c) of the STM image shown on Fig. 7(b). (Only the peak at 12 \AA is common with the two other radial distributions.) The histograms calculated by Shen *et al.*⁷ and Schaub *et al.*² reveal distances similar to the measurements presented on Fig. 11(c). Measurements shown in Fig. 11(c), in Shen *et*

*al.*⁷ and in Schaub *et al.*^{2,7} also match the histograms calculated from a model based on pseudo Mackay icosahedra (PMI) tangent to the surface (within 2-5 %)⁷ and from a model based on Bergman clusters^{19,20}. However the autocorrelation pattern and histogram calculated from Boudard's model are too dense to be compatible with Shen and Schaub's data. One can conclude from such analyses that Fig. 7(d) is the first high resolution STM image showing individual atomic features²⁵.

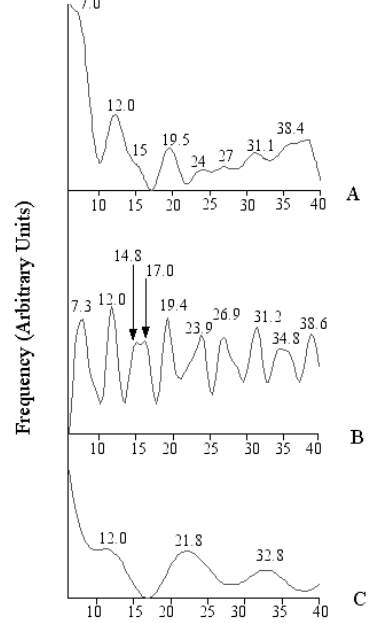


FIG. 11: Radial distributions calculated (a) from the autocorrelation pattern of Fig. 9(c) (corresponding the high resolution STM image shown on Fig. 7(d)); (b) from the autocorrelation pattern from Boudard's plane presented on Fig. 9(b) and (c) from the autocorrelation pattern calculated from the STM image shown in Fig. 7(b) (the units of the x axis are \AA).

IV. REFINED MODEL FOR THE BULK TERMINATIONS

In section II A we have derived the tilings \mathcal{T}^* , $\mathcal{T}^{*(P1)}$ and $\mathcal{T}^{*(Ns)}$ either from the ideal tiling $\mathcal{T}^{*(A_4)}$ or from their own corresponding quasilattices. We have been considering exclusively these points $q \in D_6$ that belong to the underlying tiling of the model, $\tau\mathcal{T}^{*(A_4)}$. Consequently the edge lengths in both locally derived tilings, $\mathcal{T}^{*(P1)r}$ and $\mathcal{T}^{*((Ns)r)}$ were of length $\tau^2 \mathcal{Q} = 12.553 \text{ \AA}$. If we also take into account the decoration of the tiling by Bergman/Mackay polytopes, the window for the quasilattice points of type $q \in D_6$, $W_{q_{D_6}}$ becomes the polytope derived in^{17,18,20}.

In order to consider the five-fold planes of the model \mathcal{M} , we shortly mention two important general facts that

we implicitly use in our considerations.

(i) If one icosahedrally projects to the “parallel” space, \mathbb{E}_{\parallel} (or to the “perpendicular” space, \mathbb{E}_{\perp}) the reciprocal lattice to the lattice D_6 , also known as the “weight”-lattice D_6^w , in \mathbb{E}_{\parallel} (or in \mathbb{E}_{\perp}) there appears a $\mathbb{Z}(\tau)$ -module. The module points in a plane of a three dimensional $\mathbb{Z}(\tau)$ -module in \mathbb{E}_{\parallel} , under the *-map³⁸, i. e. $\tau \rightarrow -1/\tau$, are mapped in \mathbb{E}_{\perp} into a plane too. The section of this plane in \mathbb{E}_{\perp} through the three-dimensional window (acceptance region of the three-dimensional quasilattice) is the two-dimensional window for the quasilattice in a corresponding plane in \mathbb{E}_{\parallel} . The analogous statement holds true for the line. These are the general properties of a $\mathbb{Z}(\lambda)$ module with quadratic irrationality λ . In our considerations $\lambda = \tau = (\sqrt{5}+1)/2$ and is valid for the icosahedral, five-fold, ten-fold, eight-fold and twelve-fold symmetries.

(ii) Let us consider the four translational classes with respect to the root-lattice D_6 of six-dimensional points $\frac{1}{2}(n_1, \dots, n_6) \in D_6^w$, where n_i are integers. The condition for the atomic positions $\frac{1}{2}(n_1, \dots, n_6)$ to be in a five-fold plane in \mathbb{E}_{\parallel} or \mathbb{E}_{\perp} is a class-function presented in Table I. Hence, the atomic positions in a five-fold plane of a D_6^w -icosahedrally projected $\mathbb{Z}(\tau)$ module belong to the *single* class, $q_{D_6} \equiv q, b, a$ or c .

TABLE I: The symbols e and o stand for even and odd integers, respectively. The symbol $n_{\parallel}^5 / n_{\perp}^5$ is a normal to the five-fold plane in $\mathbb{E}_{\parallel} / \mathbb{E}_{\perp}$ space, respectively. $x_{\parallel} \in \mathbb{E}_{\parallel}$ and $x_{\perp} \in \mathbb{E}_{\perp}$, where x is the point from six-dimensional space, $\mathbb{E}_{\parallel} + \mathbb{E}_{\perp}$. The scalar product is given in the units $[\kappa]$, where $\kappa = 1/[2(\tau + 2)]$.

class-criterion	class	$ n_{\parallel}^5 \cdot x_{\parallel} [\kappa]$	$ n_{\perp}^5 \cdot x_{\perp} [\kappa]$
$\frac{1}{2}(e_1, \dots, e_6); \frac{1}{2} \sum_i e_i = \text{even}$	q_{D_6}	$e + e\tau$	$e + e\tau$
$\frac{1}{2}(e_1, \dots, e_6); \frac{1}{2} \sum_i e_i = \text{odd}$	b	$e + o\tau$	$o + e\tau$
$\frac{1}{2}(o_1, \dots, o_6); \frac{1}{2} \sum_i o_i = \text{odd}$	a	$o + e\tau$	$o + o\tau$
$\frac{1}{2}(o_1, \dots, o_6); \frac{1}{2} \sum_i o_i = \text{even}$	c	$o + o\tau$	$e + o\tau$

Using the facts (i) and (ii), in the geometric model \mathcal{M} we code each five-fold plane containing a certain class of atomic positions in \mathbb{E}_{\parallel} by the five-fold cuts in \mathbb{E}_{\perp} through the *single*, to the class corresponding window W_q , W_b or W_a .

The plane of Boudard’s model on Fig. 9(b) that is consistent with the experimental measurements presented in this paper corresponds to certain planes in our model based on the $\tau\mathcal{T}^{*(2F)}$ tiling¹⁹. Fig. 12(a) schematically presents the layers of Bergman polytopes geared into each other in \mathbb{E}_{\parallel} along a five-fold axis chosen as the z -coordinate. In Fig. 12(a) the possible positions of the surface observed in Fig. 7(d) are denoted in the geometric model \mathcal{M} by L_1 - and L_2 -planes. These model-termination-planes are coded by the five-fold cuts through the window W_q on the distances of the centrum of the window $z_{\perp}^1 = 1.186$ ⑤ and $z_{\perp}^2 = 1.106$ ⑤ respectively, see Fig. 12(b). Both planes, L_1 and L_2 cut layers of Bergman polytopes of maximal density 1 in the

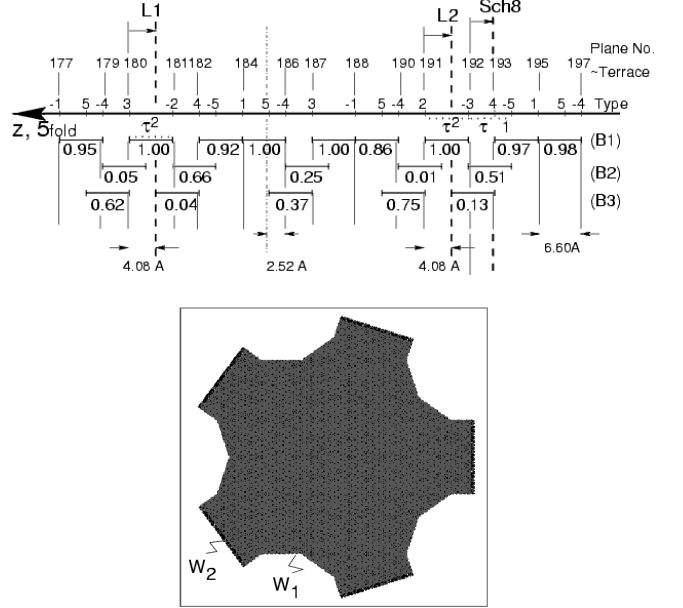


FIG. 12: (a) The layers of Bergman polytopes in \mathbb{E}_{\parallel} marked schematically along a five-fold z -axis. Below each mark for the layer is written the density of the layer relative to the maximal one. The planes of type $(\pm 1, \pm 2, \pm 3, \pm 4)$ are marked by full lines orthogonal to z -axis. They are at distances which form the Fibonacci sequence of intervals $m = 4.08 \text{ \AA}$ and $l = \tau m = 6.60 \text{ \AA}$. Only one plane of type ± 5 is marked by a pointed-dashed-line. The model planes L_1 and L_2 for the observed surface are marked by dashed lines as planes shifted from 180 and 191 (respectively) by -4.08 \AA . The biggest terrace observed by Schaub *et al.* (in their notation No. 8) which we denote by Sch8 is marked by a dashed line as a plane shifted from 192 by -4.08 \AA . (b) The windows for the quasilattice points in the model-planes L_1 and L_2 : W_2 in black and over W_2 is W_1 in grey. W_1 and W_2 are obtained as the cuts through the window $W_{q_{D_6}}$ (see Fig. 8 in Ref.²⁰) by the planes perpendicular to a five-fold axis at the heights $z_{\perp}^1 = 1.186$ ⑤ and $z_{\perp}^2 = 1.106$ ⑤, respectively. For the scale, the five-fold edge of $W_{q_{D_6}}$ is τ^{-1} ⑤. The windows W_1 and W_2 are five-fold symmetric.

model \mathcal{M} , see Fig. 12(a) and Ref.¹⁹. The cuts are situated 4.08 \AA lower into the bulk compared to the position of the model-planes numerated by 180 or 191.

A. Support of the Experimental Tiling

From the window of the plane L_1 (Fig. 13), obtained by the cut of $W_{q_{D_6}}$ at $z_{\perp} = 1.186$ ⑤, we conclude that the minimal edge length of a tiling P1 that could be derived from the subset of points in the plane is $\tau\mathcal{T} = 7.8 \text{ \AA}$, in agreement with the observed tiling on the surface, see Fig. 9(a). If the quasilattice points of the class a were determining the tiling on the surface, the minimal edge length would have been $\tau^2 \mathcal{T} = 12.553 \text{ \AA}$, and if it were the class b , the minimal edge length could be even \mathcal{T}

$= 4.795 \text{ \AA}$. The windows W_b is on the Fig. 8(b) of Ref.²⁰ and the window W_a in Refs.^{17,18}. With the plane L_2 we would evidently draw the same conclusion for the edge length (Figs. 12(b) and 13).

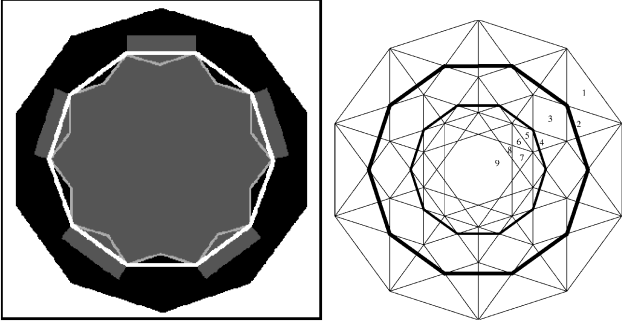


FIG. 13: (a) A window for the tiling on the surface in grey as obtained by cutting the window W_{qD_6} perpendicular to a five-fold axis at a height $z_{\perp} = 1.186 \text{ \AA}$ ⑤. The window is five-fold symmetric. For the scale, the window for $\tau^{-1}\mathcal{T}^{*(A_4)}$ is shown in black in the background. The window for \mathcal{T}^* with edge length ② is inscribed by thin white lines. The window for the tiling $\mathcal{T}^{*(P1)}$ with edge length ② by thick white lines. This window is not completely inside of the grey window for the plane, hence, the tiling $\mathcal{T}^{*(P1)}$ of edge length ② cannot be derived from the point set in the plane. (b) In the window for $\mathcal{T}^{*(A_4)}$ two concentric windows for $\mathcal{T}^{*(P1)}$ tilings are inscribed by thick black lines. The smaller window (by the factor $\tau^{(-1)}$) corresponds to the tiling $\mathcal{T}^{*(P1)}$ with the shortest possible edge length $\tau 2$ to be reconstructed from the point set of the observed plane. This window is completely within the grey window of the plane. The edge length of the corresponding tiling, 7.8 \AA matches the one of experimental tiling in Fig. 9(a).

We may propose our method by considering how to reproduce an experimental tiling under the assumption that the model \mathcal{M} is a good description of i-AlPdMn. The rule is: estimate which plane from the model corresponds to the surface being observed and determine the coding window for the set of quasilattice points for the model-plane. If one wishes to reconstruct some of the tilings \mathcal{T}^* , $\mathcal{T}^{*(P1)}$, $\mathcal{T}^{*(N_s)}$ or the covering $\mathcal{C}_{\mathcal{T}^{*(A_4)}}$ with the shortest edge, then search for the biggest of the corresponding windows that is (tightly) contained in the window of the estimated model-plane. From this knowledge the edge length of the tiling can be determined and an attempt made to reconstruct it.

B. Atomic Densities of Terminations

We recall that the observed dark pentagonal holes in the terraced surfaces imaged by Schaub *et al.* that we considered in¹⁹ were bigger by a factor τ than the concave surfaces of Bergman polytopes. Whereas the edge of the Bergman face in \mathcal{M} is 3.0 \AA , the edge of the dark pentagonal hole was circa 4.8 \AA . In Ref.¹⁹ we considered

the model terminations to be the model planes attached to the upper surfaces of the Bergman polytopes in the most dense layers. Now, with the high resolution STM image in Fig. 7(d), we conclude that the model-planes that represent the terraces and are related to the most dense layers of Bergman polytopes¹⁹ should be shifted by -4.08 \AA deeper into the direction of the bulk. On these positions the dark pentagonal holes of Schaub *et al.* are of the same size as the “lower equatorial” pentagon (lower in the z -direction, with respect to the bulk, see Fig. 12(a)) of the Bergman decoration. The edge length of that decagon is exactly 4.8 \AA . The surface observed in this paper (L_2) corresponds to the second biggest terrace of Schaub (labelled No. 7 in their work)⁴. The new model bulk-terminations are cutting the densest layers of the Bergman polytopes. What about the atomic densities of these new bulk-terminations?

For the atomic density of a surface termination, Gierer *et al.*¹⁴ consider the sum of densities of two atomic layer-planes at the surface, separated by 0.48 \AA . Their value averaged over the measured terminations is $0.136 \text{ atoms per \AA}^2$.

TABLE II: We calculate the densities on *old* and *new* (shifted by -4.08 \AA) positions of the terminations. Following Gierer *et al.* for each termination we calculate the densities of two atomic layer-planes, one on the surface, the q -plane, and another shifted by -0.48 \AA , the b -plane: $\rho_{No}^{old}\{q(No) + b(No - 0.48 \text{ \AA})\}$, $\rho_{No}^{new}\{q(No - 4.08 \text{ \AA}) + b(No - 4.08 \text{ \AA} - 0.48 \text{ \AA})\}$.

No	180	191	192	average
$\rho_{No}^{old}[\text{\AA}^{-2}]$	0.131	0.129	0.093	0.118
$\rho_{No}^{new}[\text{\AA}^{-2}]$	0.137	0.136	0.135	0.136

In Table II we list the values of densities ρ_{No} of terminations on three different positions labelled by the No of the reference plane in our geometric model \mathcal{M} . We list the values of densities at *old*¹⁹ and *new* (shifted by -4.08 \AA) positions of the terminations. Under the surface termination, following Gierer *et al.*¹⁴ we consider the two-layer-plane configuration in which the planes are separated by -0.48 \AA . From Table II it is evident that the densities of terminations related to the “new” positions shifted by -4.08 \AA are in much better agreement with the LEED data of Gierer *et al.*¹⁴. The value of average density of the new terminations is higher than of the old ones¹⁹, although the q -planes alone are clearly more dense at the old than at the new positions.

V. CONCLUSIONS

We have presented an atomically resolved, high resolution STM image of a flat terrace of the five-fold $\text{Al}_{70}\text{Pd}_{21}\text{Mn}_9$ surface. Based on this image we deduced that the five-fold model-termination plane should be placed 4.08 \AA lower than in¹⁹. At the new positions of model-termination planes the dark pentagonal holes^{2,4,19}

are of appropriate size, they fit to the model: the new surface plane is placed in the cut through the most dense Bergman layer in the model. The average atomic density in the new terminations is in agreement with the LEED measurements of Gierer *et al.*¹⁴. The edge length of an experimentally derived tiling of the surface by the prototiles of the Penrose P1 tiling (based on pentagons of height equal to $12 \pm 0.36 \text{ \AA}$) is shown to be in agreement

with the bulk model \mathcal{M} based on the tiling $\tau\mathcal{T}^{*(2F)}$ ¹⁹.

The EPSRC (Grant numbers GR/N18680 and GR/N25718), NSF (Grant number DMR-9819977) and DFG (Grant number KA 1001/4-2) are acknowledged for funding.

¹ A.R. Kortan, R.S. Becker, F.A. Thiel, and H.S. Chen, Phys. Rev. Lett. **64**, 200 (1990).

² T. M. Schaub, D. E. Bürgler, H.-J. Güntherodt, and J.-B. Suck, Phys. Rev. Lett. **73**, 1255 (1994).

³ T. M. Schaub, D. E. Bürgler, C. Schmidt, H.-J. Güntherodt, and J.-B. Suck, Z. Phys. B **96**, 93 (1994).

⁴ T. M. Schaub, D. E. Bürgler, H.-J. Güntherodt, J.-B. Suck, and M. Audier, Appl. Phys. A **61**, 491 (1995).

⁵ T. M. Schaub, D. E. Bürgler, C. Schmidt, and H.-J. Güntherodt, J. Non-Cryst. Solids **205/207**, 748 (1996).

⁶ Ph. Ebert, F. Yue, and K. Urban, Phys. Rev. B **57**, 2821 (1998).

⁷ Z. Shen, C. R. Stoldt, C.J. Jenks, T. A. Lograsso, and P. A. Thiel, Phys. Rev. B **60**, 14688 (1999).

⁸ J. Ledieu, A. Munz, T. Parker, R. McGrath, R. D. Diehl, D. W. Delaney, and T. A. Lograsso, Surface Science **433/435**, 665 (1999).

⁹ J. Ledieu, A. Munz, T. Parker, R. McGrath, R. D. Diehl, D. W. Delaney, and T. A. Lograsso, Mat. Res. Soc. Symp. Proc. **553**, 237 (1999).

¹⁰ D. Naumović, P. Aebi, L. Schlapbach, and C. Beeli, *New Horizons in Quasicrystals: Research and Applications* (A.I. Goldman, D.J. Sordelet, P.A. Thiel and J.M. Dubois (World Scientific), Singapore, 1997).

¹¹ D. Naumović, P. Aebi, L. Schlapbach, C. Beeli, T. A. Lograsso, and D. W. Delaney, *Proceedings of the 6th International on Quasicrystals (ICQ-6, Yamada Conference XLVII)* (S. Takeuchi and T. Fujiwara (World Scientific) Singapore, 1998).

¹² D. Naumović, P. Aebi, C. Beeli, and L. Schlapbach, Surface Science **433-435**, 302 (1999).

¹³ M. Gierer, M.A. Van Hove, A.I. Goldman, Z. Shen, S.-L. Chang, C.J. Jenks, C.-M. Zhang, and P.A. Thiel, Phys. Rev. Lett. **78**, 467 (1997).

¹⁴ M. Gierer, M.A. Van Hove, A.I. Goldman, Z. Shen, S.-L. Chang, P.J. Pinhero, C.J. Jenks, J.W. Anderegg, C.-M. Zhang, and P.A. Thiel, Phys. Rev. B **57**, 7628 (1998).

¹⁵ M. Boudard, M. de Boissieu, C. Janot, G. Heger, C. Beeli, H.-U. Nissen, H. Vincent, R. Ibberson, M. Audier, and J. M. Dubois, J. Phys.: Cond. Matter **4**, 10149 (1992).

¹⁶ V. Elser, *Phil. Mag.* **B73**, 641 (1996).

¹⁷ P. Kramer, Z. Papadopoulos, and W. Liebermeister, in *Proc. of 6th Int. Conf. on Quasicrystals, Yamada Conference XLVII*, edited by S. Takeuchi and T. Fujiwara, p.71 (World Scientific, Singapore, 1998).

¹⁸ Z. Papadopoulos, P. Kramer, and W. Liebermeister, in *Proc. of the Int. Conf. on Aperiodic Crystals, Aperiodic 1997*, edited by Marc de Boissieu, Jean-Louis Verger-Gaugry, and Roland Currant, p. 173 (World Scientific, Singapore, 1998).

¹⁹ G. Kasner, Z. Papadopoulos, P. Kramer, and D. E. Bürgler, Phys. Rev. B **60**, 3899 (1999).

²⁰ Z. Papadopoulos, P. Kramer, G. Kasner, and D. Bürgler, Mat. Res. Soc. Symp. Proc. **553**, 231 (1999).

²¹ P. Kramer, Z. Papadopoulos, and H. Teuscher, J. Phys.: Condens. Matter **11**, 2729 (1999).

²² D. S. Rokhsar, N. D. Mermin and D. C. Wright, Phys. Rev. B **35** 5487 (1987).

²³ P. Kramer, Z. Papadopoulos, and D. Zeidler, in *Symmetries in Science V: Algebraic structures, their representations, realizations and physical applications*, edited by B. Gruber and L. C. Biedenharn, p. 395 (Plenum, New York, 1991).

²⁴ A. Katz, and D. Gratias, in *Proceedings of the 5th International Conference on Quasicrystals*, edited by C. Janot and R. Mosseri p. 164 (World Scientific, Singapore, 1995).

²⁵ J. Ledieu, R. McGrath, R.D. Diehl, T.A. Lograsso, D.W. Delaney, Z. Papadopoulos and G. Kasner, Surface Science **492/3** L729 (2001).

²⁶ J.H. Conway and N.J.A. Sloane, *Sphere Packings, Lattices and Groups* (Springer, New York 1988)

²⁷ M. de Boissieu, P. Stephens, M. Boudard, C. Janot, D. L. Chapman, and M. Audier, J. Phys.: Condens. Matter **6**, 10725 (1994).

²⁸ M. Baake, P. Kramer, M. Schlottmann, and D. Zeidler, Int. J. Mod. Phys. B **4**, 2217 (1990).

²⁹ Z. Papadopoulos, C. Hohneker, and P. Kramer, Discrete Math. **221**, 101 (2000).

³⁰ K. Edagawa, K. Suzuki, and S. Takeuchi, Phys. Rev. Lett. **85**, 1674 (2000).

³¹ P. Kramer, J. Phys. A **32**, 5781 (1999).

³² P. Kramer, Mat. Sci. Eng. A **294-296** 401 (2000).

³³ Z. Papadopoulos and G. Kasner, *Coverings and tilings derived from the class of tilings $\mathcal{T}^{*(A_4)}$, covering of $\mathcal{T}^{*(2F)}$* in *Coverings of Discrete Quasiperiodic Sets, Theory and Applications to Quasicrystals*, Edit. P. Kramer, Z. Papadopoulos to be published by Springer, Berlin 2002.

³⁴ B. Grünbaum and G.C. Shepard, *Tilings and Patterns*, W.H. Freeman, San Francisco, 1987.

³⁵ K. Niizeki, J. Phys. A: Math. Gen. **22**, 4281 (1989).

³⁶ D.W. Delaney, T.E. Bloomer, and T.A. Lograsso, *New Horizons in Quasicrystals: Research and Applications* (eds. A.I. Goldman, D.J. Sordelet, P.A. Thiel and J.M. Dubois (World Scientific), Singapore, 1997).

³⁷ C. Jenks, D.W. Delaney, T.E. Bloomer, S.-L. Chang, T.A. Lograsso, Z. Shen, C.-M. Zhang, and P.A. Thiel, Appl. Surf. Sci. **103**, 485 (1996).

³⁸ R. V. Moody in: *The Mathematics of Long-Range Aperiodic Order*, ed. R. V. Moody, p. 403 Kluwer (1997).

³⁹ Bergman polytope is a dodecahedron with particular concave pentagonal faces, see Ref.¹⁶.

⁴⁰ These prototiles can be uniquely reconstructed from the point set of atomic positions.